Phase diagram, energy scales, and nonlocal correlations in the Anderson lattice model

D. Tanasković, K. Haule, G. Kotliar, and V. Dobrosavljević

Phys. Rev. B **84**, 115105 — Published 9 September 2011

DOI: 10.1103/PhysRevB.84.115105

Phase diagram, energy scales and nonlocal correlations in the Anderson lattice model

D. Tanasković,[1] K. Haule,[2] G. Kotliar,[2] and V. Dobrosavljević[3]

[1]*Scientific Computing Laboratory, Institute of Physics Belgrade, University of Belgrade, Pregrevica 118, 11080 Belgrade, Serbia*
[2]*Department of Physics and Astronomy, Rutgers University, Piscataway, New Jersey 08854, USA*
[3]*Department of Physics and National High Magnetic Field Laboratory, Florida State University, Tallahassee, Florida 32306, USA*

We study the Anderson lattice model with one f-orbital per lattice site as the simplest model which describes generic features of heavy fermion materials. The resistivity and magnetic susceptibility results obtained within dynamical mean field theory (DMFT) for nearly half-filled conduction band show the existence of a single energy scale T^* which is similar to the single ion Kondo temperature T_K^o. To determine the importance of inter-site correlations, we have also solved the model within cellular DMFT (CDMFT) with two sites in a unit cell. The antiferromagnetic region on the phase diagram is much narrower than in the single-site solution, having smaller critical hybridization V_c and Néel temperature T_N. At temperatures above T_N the nonlocal correlations are small, and the DMFT paramagnetic solution is in this case practically exact, which justifies the ab initio LDA+DMFT approach in theoretical studies of heavy fermions. Strong inter-site correlations in the CDMFT solution for $T < T_N$, however, indicate that they have to be properly treated in order to unravel the physical properties near the quantum critical point.

PACS numbers: 71.27.+a,71.30.+h

I. INTRODUCTION

Heavy fermions have been intensively studied in the last thirty years and large amount of experimental data has been gathered,[1,2] but a complete microscopic theory of these materials is still not available.[3] The unusual low temperature properties originate from the electrons from partially field f-shells which hybridize with a broad band of weakly interacting conduction electrons. At high temperatures, the f-electrons are weakly coupled to the conduction electron band and act as local magnetic moments on which the conduction electrons are scattered. Below the characteristic temperature (the lattice coherence temperature) T^*, the coherent quasiparticles start to develop and the resistivity suddenly decreases. The dependence of T^* on microscopic parameters and the nature of the coherent heavy electron (Kondo) liquid is still a subject of active debate.[4–6]

Many experiments clearly show the existence of a unique energy scale that characterizes all transport and thermodynamic properties[7,8] and several attempts were made to explain universal features of heavy fermions, both within the phenomenological theory[4,5] and from the solution of the microscopical model.[9] There is, however, a growing evidence[6] that the energy scales which dominate the low temperature properties of heavy fermions depend on details of the density of states near the Fermi level and the degeneracy and crystal fields splitting of the f states - the system dependent properties which cannot be captured by the simple theoretical model with just one f-spin dublet or a featureless conduction band density of states. The physics is even richer at temperatures $T \ll T^*$, where the system typically orders magnetically and even exhibits superconductivity.[10–12]

In this work we solve the Anderson lattice model (ALM) with one f-electron orbital per lattice site, in order to precisely determine the lattice coherence temperature T^* and the importance of nonlocal correlations in different regions of the phase diagram. We concentrate on the most interesting regime of parameters near the antiferromagnetic phase driven by the conduction electron mediated Ruderman-Kittel-Kasuya-Yosida (RKKY) interaction.[13] The model is first solved within the DMFT approximation[14] which is exact in the case of purely local correlations, i.e. in the case where the self-energy depends only on frequency and not on the momentum. The relevance of the local approximation is tested by a comparison with the CDMFT solution.[15,16] We consider a cluster of two sites in a self-consistently determined medium as a minimal model which treats the inter-site correlations beyond the mean field level. For temperatures larger than the Néel temperature, we find that the nonlocal correlations are very small and the local DMFT solutions becomes practically exact. Therefore, for stronger hybridization the lattice coherence temperature is determined by the local DMFT solution and in this case, in the ALM close to half-filling, we find that it is proportional to the single ion Kondo temperature for the same set of parameters, $T^* \approx T^*_{DMFT} \sim T_K^o$. For weaker hybridization, near the antiferromagnetic critical point, $T^*_{DMFT} \lesssim T_N$ and the coherence temperature is likely to be dominated by the inter-site correlations driven by the RKKY interaction. To determine the precise form of T^* in this regime and to unravel the physical properties near the quantum critical point, we need to consider larger clusters and different clustering schemes. The important conclusion can, however, be drawn already from the present results: for temperatures $T > T_N$ the correlations are local, which means that LDA+DMFT theory gives an excellent framework for a quantitative study of heavy fermion ma-

terials in this temperature range.[17–19] The LDA+DMFT method,[20] obtained by combining DMFT with the local density approximation (LDA) treats on equal footing the band structure, the atomic multiplet splitting and the Kondo physics, but assumes that the correlations are local in space. This method has led to a significant progress in the study of strongly correlated materials, and may also prove crucial in order to determine the importance of the crystal field effects and atomic multiplets for low temperature properties of various heavy fermions.

The remaining part of the paper is organized as follows. In Section II we define the Hamiltonian and describe the CDMFT method of its solution. Section III contains the phase diagram and a comparison of the results with a single-site DMFT. The coherence temperature T^*_{DMFT} is determined from the magnetic susceptibility and resistivity results in Section IV, and in Section V the strength of nonlocal correlations is examined. Conclusions and discussion are presented in Section VI.

II. METHODS

We consider the periodic Anderson model of three-dimensional cubic lattice given by the Hamiltonian

$$\begin{aligned} H &= -t\sum_{\langle ij\rangle,\sigma} c^\dagger_{i\sigma}c_{j\sigma} - \mu\sum_{i\sigma} c^\dagger_{i\sigma}c_{i\sigma} + V\sum_{i\sigma}(f^\dagger_{i\sigma}c_{i\sigma} + \text{h.c.}) \\ &+ (E_f-\mu)\sum_{i\sigma} f^\dagger_{i\sigma}f_{i\sigma} + U\sum_i n^f_{i\uparrow}n^f_{i\downarrow}. \end{aligned} \tag{2.1}$$

$c^\dagger_{i\sigma}$ and $f^\dagger_{i\sigma}$ create a conduction band electron (c-electron) and f-electron at site i for spin σ. $n^f_{i\sigma} = f^\dagger_{i\sigma}f_{i\sigma}$ is the occupation number operator of f-electrons, t nearest neighbor hopping amplitude, μ chemical potential, V hybridization strength, U interaction, and E_f is f-electron energy level. In DMFT, the solution of the ALM reduces to solving a single impurity problem supplemented by a self-consistency condition.[14] In CDMFT, in contrast, the original lattice is tiled with a superlattice of clusters. An effective Anderson impurity action is derived for a single cluster and supplemented by the self-consistency condition which relates the cluster Green's function to the local Green's function of the superlattice.[15,16] For the cluster of two impurities, allowing for the antiferromagnetic order, there are three independent components of the cluster Green function, e.g. $G_{11\uparrow}$, $G_{22\uparrow}$, and $G_{12\uparrow}$. Details of the self-consistent procedure for calculation of Green's function are presented in Appendix A.

Technically the most difficult step in the DMFT (CDMFT) procedure is a solution of the model of an impurity (cluster of impurities) immersed into the given conduction bath. For this step we use the Continuous Time Quantum Monte Carlo (CTQMC) impurity solver[21] in the implementation from Ref. 22. This allows us to obtain numerically exact solution even at very low temperatures which are well below the Néel temperature of the model. We note that the same model in the CDMFT framework was studied previously, but this work used numerical methods which are inferior as compared to the CTQMC. The CTQMC allows us to reach temperatures order of magnitude lower than the Hirsh-Fye impurity solver used in Ref. 23. The exact diagonalization method,[24] on the other hand, is restricted to zero temperature, it discretizes the degrees of freedom of the conduction bath and uses a discrete mesh of frequency points much larger than the temperature in our work. Since the energy scales for the range of parameters where the Kondo temperature and RKKY interaction energy are comparable in magnitude are very small, the numerical method that we use in this paper is crucial in order to precisely determine the phase diagram and to examine the importance of nonlocal correlations.

III. PHASE DIAGRAM

We present the solution of DMFT (CDMFT) equations for the Anderson lattice model for $U = 1.2$, $E_f = -0.4$, $\mu = -0.03$ and various hybridization V. These parameters correspond to metallic nearly half-filled system, where stable magnetic phase and strong nonlocal effects are expected. The occupation of f-electrons is close to 1 (Kondo limit) and the total occupation close to 2. Nearly half-filled conduction band leads to antiferromagnetic correlations in the spin density. We will concentrate on the most interesting regime of hybridization where the Kondo temperature and RKKY interaction energy are of the same order of magnitude. The energy will be measured in units of the conduction electron half-bandwidth $D = 6t = 1$. The lowest temperature in numerical results is $T = 1/1200$ which is crucial in order to stabilize the antiferromagnetic solution within CDMFT.

The phase diagram of the model is shown in Fig. 1. The phase boundary between the antiferromagnetic (AFM) and paramagnetic solution is determined by the relative strength of the Kondo screening and RKKY interaction. The result is in a qualitative agreement with Doniach's phase diagram: the AFM solution is stabilized for small hybridization V when $J_{RKKY} \sim \rho_o {J^o_K}^2$ dominates over the Kondo scale $T^o_K \sim \exp(-1/2\rho_o J^o_K)$. Here $J^o_K = (\frac{1}{|E_f-\mu|} + \frac{1}{|U+E_f-\mu|})V^2$ is the bare Kondo coupling and ρ_o is the density of states of the conduction electrons at the Fermi level. The numerical solution of ALM model, however, gives us a possibility to *quantitatively* determine the relevant energy scales. Red dotted line in Fig. 1 is the lattice coherence temperature T^*_{DMFT} obtained, in DMFT solution, as the temperature corresponding to the maximum resistivity for a given value of V (see Section IV). In DMFT, which neglects nonlocal correlations, the Néel temperature T_N^{DMFT} can be taken as the measure of J_{RKKY}. In AFM phase $T^*_{DMFT} < T_N^{DMFT}$ in almost entire phase diagram (except very close to the critical V_c^{DMFT}), in agreement

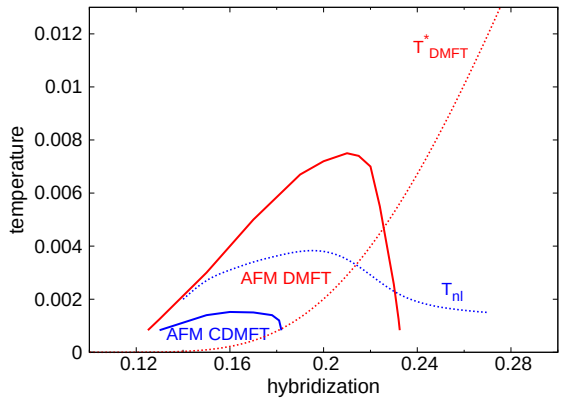

FIG. 1: (Color online) Temperature vs. hybridization phase diagram in DMFT (full red line) and CDMFT (full blue line). Red dotted line is the coherence temperature in the DMFT solution. Nonlocal correlations are very weak for temperatures above T_{nl} (blue dotted line) and in this region the paramagnetic DMFT solution is practically exact.

with recent DMFT phase diagram for the Kondo lattice model.[25]

The AFM region in the CDMFT solution is significantly narrower than in the single site DMFT solution due to the inter-site correlations which are treated beyond the mean-filed level in CDMFT. The highest Néel temperature in CDMFT is approximately four times lower than in DMFT. The critical hybridization V_c for the quantum phase transition reduces from $V_c^{DMFT} \approx 0.23$ in DMFT to $V_c \approx 0.18$ in CDMFT solution. As examined in detail in Section V, above the temperature $T_{nl} \sim 0.004$ the nonlocal correlations are very small and the paramagnetic solution in single-site DMFT becomes practically exact for $T \gtrsim T_{nl}$. For $T < T_{nl}$, however, inter-site correlations found in two-site CDMFT are strong and dominate the low temperature physics of the ALM for $V \lesssim V_c$.

The CTQMC impurity solver[22] enables us to stabilize the AFM solution in CDMFT at very low temperatures with small minus sign problem. The numerical quality of the data can be verified from the magnetization results shown on Fig. 2. In the DMFT solution, the mean-field behavior of the staggered magnetization, $n_{f\uparrow} - n_{f\downarrow} \propto -(n_{c\uparrow} - n_{c\downarrow}) \propto (1 - T/T_c)^{1/2}$, is observed in a wide temperature range. In the CDMFT solution, the short range correlations are better taken into account and the mean-field behavior is restricted to narrower temperature region near T_c. The error bars are the statistical errors estimated from several CTQMC runs. They are much larger in the CDMFT solution due to the appearance of minus sign problem in AFM phase. The staggered magnetization $m_f = n_{f\uparrow} - n_{f\downarrow}$ is less than 1 even as $T \to 0$ due to the hybridization with the conduction electrons. m_f in CDMFT solution is almost two times smaller than in DMFT. Typical results for the self-energy and Green's functions on the Matsubara axis are shown in Appendix B.

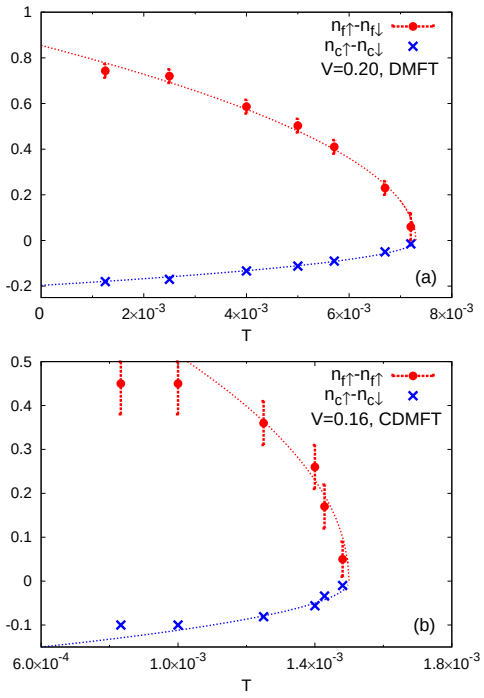

FIG. 2: (Color online) Staggered magnetization of f- and c-electrons in DMFT (a) and CDMFT solution (b). Dotted lines are fit to the square root mean-field curve.

IV. COHERENCE TEMPERATURE IN DMFT SOLUTION

At high temperatures f-electrons are weakly coupled to the conduction band electrons and behave as local moments. The scattering of c-electrons initially increases with decreasing temperature similarly as in the limit of diluted magnetic moments. The resistivity reaches a maximum at a characteristic temperature T_{max} that can be taken for a definition of the lattice coherence temperature. Below T_{max} f- and c-electrons strongly hybridize and eventually form long-lived heavy quasiparticles.

In the single-site DMFT it is easy to calculate the scattering rate and the resistivity. They are obtained from the self-energy Σ_c which corresponds to the conduction electrons. The conduction electrons Green function is given by $G_c(\omega) = \frac{1}{N}\sum_{\vec{k}}[\omega + \mu - \varepsilon_{\vec{k}} - \Sigma_c(\omega)]^{-1}$, where $\Sigma_c(\omega) = V^2/(\omega - E_f + \mu - \Sigma_f(\omega))$, and Σ_f is the self-energy of the impurity (i.e. f-electron). The scattering rate is given by $\tau^{-1} = -2\mathrm{Im}\Sigma_c(\omega = 0)$, and the resistivity ρ is obtained from the zero frequency limit of the real part of the optical conductivity,[26,27] $\rho = 1/\mathrm{Re}\,\sigma(\omega \to 0)$,

$$\rho^{-1} = \pi e^2 \frac{1}{N} \sum_{\vec{k}} \int d\omega \left(-\frac{df}{d\omega}\right) v_x^2 A^2(\vec{k}, \omega). \qquad (4.1)$$

Here $A(\vec{k}, \omega) = \mathrm{Im}(\omega + \mu - \varepsilon_{\vec{k}} - \Sigma_c(\omega))$ is the conduction electron spectral function, $v_x = \partial\varepsilon_{\vec{k}}/\partial k_x$, N is the num-

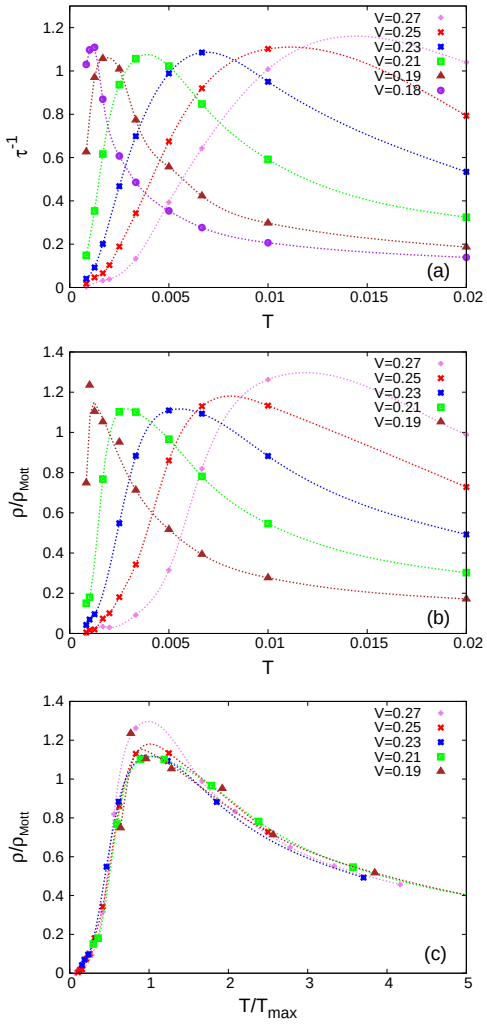

FIG. 3: (Color online) (a) Scattering rate and (b) resistivity as a function of temperature for several hybridization strengths. (c) The resistivity curves approximately collapse to a single one after scaling the temperature.

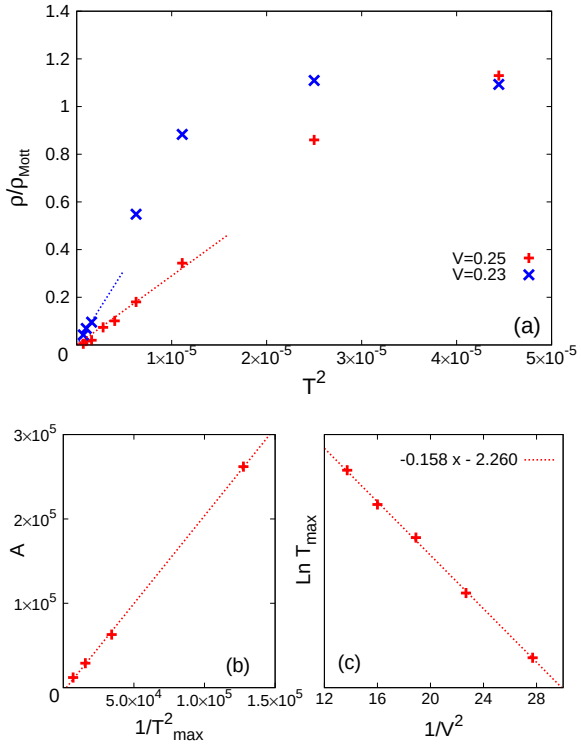

FIG. 4: (Color online) (a) Resistivity as function of T^2. Linear region is observed for $T \lesssim T_{max}/2$. (b) The resistivity slope A is linear function of $1/T_{max}^2$. (c) Temperature T_{max} of the resistivity maximum depends exponentially on the hybridization.

ber of $\vec{k}$ states in the Brillouin zone, and f is the Fermi-Dirac distribution. In the CTQMC impurity solver the self-energy is obtained at Matsubara frequencies and to obtain the real frequency data we assume the polynomial form for Σ_c at low frequencies, $\Sigma_c = az^2 + bz + c$, and determine complex parameters a, b, and c from the real and imaginary parts of $\Sigma_c(i\omega_n)$ for first three Matsubara frequencies, for each T and V. This simple analytical continuation is not restricted to the Fermi liquid region and it turned out to be remarkably accurate as we will see from the analysis of the resistivity curves.

The scattering rate is shown on Fig. 3(a) as a function of temperature and for several values of hybridization parameter. The scattering rate curves have a prominent maxima at values which are of the order of the Mott-Ioffe-Regel limit for maximal metallic resistivity, $\tau_{max}^{-1} \sim 1$. The resistivity saturation at this value, which corresponds to the mean free path of one lattice spacing, is indeed the property of heavy fermions.[28,29] It can be simply explained from the sum rule, and the resistivity saturates when the Drude peak in the optical conductivity gets completely smeared with increasing temperature.[30] The resistivity curves, Fig. 3(b), have the same form as the scattering rate curves, with only slightly shifted maxima due to the temperature dependence of the real part of Σ_c. The resistivity is given in units of ρ_{Mott} defined as the resistivity for $\tau^{-1} = 1$. When the temperature is scaled with T_{max}, the shape of the resistivity curves is almost the same for all values of the hybridization strength, Fig. 3(c).

The resistivity, Fig. 4(a), follows the Fermi liquid form, $\rho = AT^2$, up to the temperature $\sim T_{max}/2$ which can be taken as the boundary of the Fermi liquid region. We use the data for $T < T_{max}/2$ to determine the slope A, which depends linearly on $1/T_{max}^2$, Fig. 4(b). This is a manifestation of the Kadowaki-Woods relation[7,31,32] which establishes a universal ratio between the resistivity and thermodynamic quantities, like the specific heat. In our case $A \sim 1/T_{max}^2 \sim m^{*2} \sim \gamma^2$, where m^* is the effective mass and γ the specific heat coefficient. The Kadowaki-Woods ratio explains excellent scaling of the

resistivity curves at low temperatures. By scaling only the temperature, we find that the curves approximately collapse to a single curve in the whole temperature range since the maximum resistivity is approximately the same for all values of hybridization. The resistivity scaling was successfully applied in early experimental paper on $CeCu_6$.[8]

The resistivity scaling clearly shows the existence of just one energy scale - lattice coherence temperature $T^* \equiv T_{max}$. Therefore, it is very important to determine its dependence on microscopic parameters and make a comparison with the single ion Kondo temperature. As we show on Fig. 4(c), the resistivity maximum depends exponentially on the hybridization parameter. We can use a relation $T^* = C\exp(-1/2\rho_o J_K^{latt})$ as a definition for the *lattice Kondo coupling*. Taking $\rho_o = 0.855$ for the conduction band density of states, we obtain $J_K^{latt} = 3.7V^2 \approx J_K^o$, where $J_K^o = (\frac{1}{|E_f-\mu|} + \frac{1}{|U+E_f-\mu|})V^2 = 3.9V^2$. Therefore, in the theory with only local correlations, the coherence temperature has the same functional form as the single ion Kondo temperature T_K^o and the effective Kondo coupling J_K^{latt} is approximately the same as J_K^o. We note that the functional form of $T_{max}(V)$ is the same if T_{max} is taken from the scattering rate curves, with the same value for J_K^{latt} and with the prefactor C only slightly smaller than the one obtained from the resistivity curves.

We further compare the lattice and single ion energy scale using the magnetic susceptibility data. Static local magnetic susceptibility, $\chi_{loc}(\omega = 0) \equiv \chi$, can be determined very accurately using CTQMC as the impurity solver and does not require analytical continuation of the data. The plots on Fig. 5 are obtained by scaling with a single parameter T_o - which we call *the lattice Kondo temperature*. As in the single ion case, the temperature is scaled by T_o and the susceptibility is multiplied by T_o in order to collapse the data on a single curve. T_o has exponential dependence on V^2 as we analyze in detail in the rest of this Section. The scaling of the susceptibility, Fig. 5(a), is very good except for the temperatures $T < T_{max}$. The reason is that the hybridization bath assumes strong temperature dependence for temperatures lower than the lattice coherence temperature. If we omit the data in the scaling analysis for $T < T_{max}$ for each value of V, we find that all the data collapse to a single universal curve, inset in Fig. 5(a). The same scaling analysis for the inverse susceptibility is shown in Fig. 5(b).

We now carefully analyze the local susceptibility and make a comparison with the single ion case. Fig. 6(a) and Fig. 6(b) show the inverse susceptibility as a function of temperature for the ALM and the single impurity Anderson model (SIAM). We start from the Curie-Weiss form

$$\chi^{-1} = aT + bT_o. \qquad (4.2)$$

Here a and b are constants. In the single ion case T_o corresponds to the Kondo temperature T_K^o. In the lattice model $\chi(T)$ also follows the Curie-Weiss form except

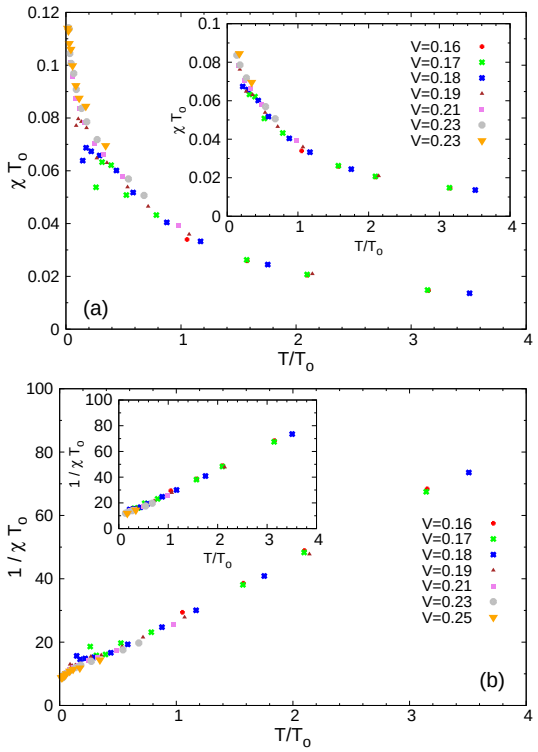

FIG. 5: (Color online) Scaled susceptibility (a) (inverse susceptibility (b)) as a function of scaled temperature. If we omit the data for $T < T_{max}$ (the insets), the scaling is excellent.

at the lowest temperatures, $T \lesssim T_{max}$, where it significantly deviates from linear dependence. The inverse susceptibility at $T = T^* = T_{max}$ is shown by full red dots in Fig. 6(a). As expected, the value of χ^{-1} at $T = T^*$ is proportional T^*. To obtain the lattice Kondo temperature T_K^{latt}, we omit the data for $T < T^*$ and make a fit to Eq. (4.2). For the case of a single impurity we can keep all data to obtain $T_o \equiv T_K^o$. The ALM and SIAM values for T_o differ by a factor two, Fig. 6(c), but have the same exponential dependence on V^2, Fig. 6(d): $T_o \propto \exp(-1/2\rho_o J_K)$, where the lattice Kondo coupling $J_K^{latt} \approx J_K^o \propto V^2$. Some deviation from linear behavior for SIAM is due to the small change of the occupation number ($0.9 < n_f < 0.96$) since we keep the chemical potential fixed while changing T and V.

We can conclude that both the resistivity and magnetic susceptibility data give the same value for the effective lattice Kondo coupling whose value is very similar to the bare Kondo coupling in the the case of diluted impurities. The Curie-Weiss form, Eq. (4.2), gives the value of T_o up to the prefactor. In order to compare the absolute values of $T^* \equiv T_{max}$ and $T_K^{latt} \equiv T_o$ for the ALM, we can use the value b from the single impurity theory. From the Wilson formula[1] $\chi(T = 0) = 0.4128/(4T_K^o)$, which gives $b = 9.7$. (We used $b = 9.7$, $a = 4$, and $g\mu_B = 1$ on the scaling plot, Fig. 5.) Then $T^*/T_K^{latt} = 0.6$ and their ratio does not depend on V. The conclusion that T^* and T_K^o

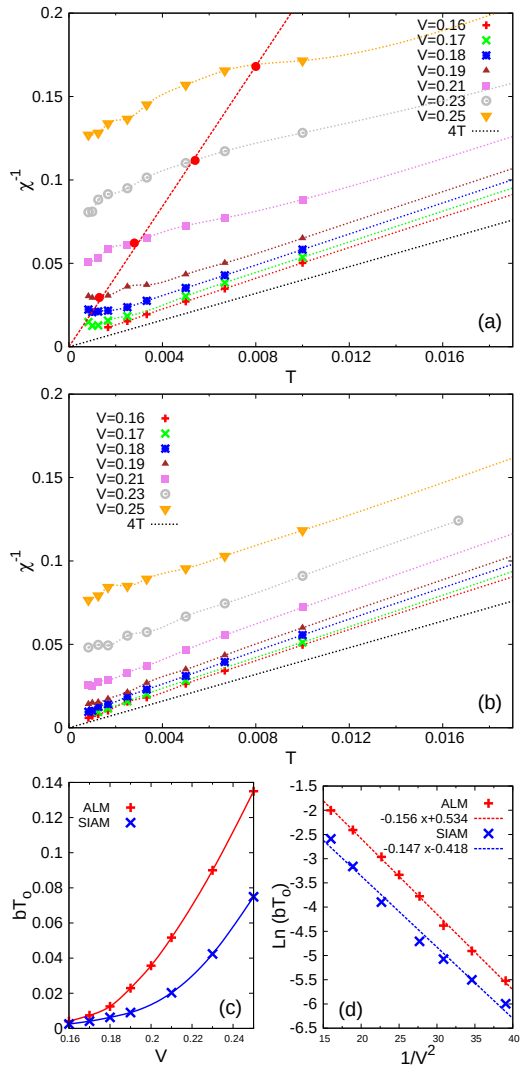

FIG. 6: (Color online) Inverse magnetic susceptibility as a function of temperature for ALM (a), and SIAM (b). For the ALM the susceptibility follows the Curie-Weiss form above T^* (full red dots). The Curie-Weiss temperature for ALM is approximately twice larger than in SIAM, panel (c), but has the same functional dependence on hybridization, panel (d).

have the same exponential dependence on the hybridization parameter, i.e. on the coupling constant, agrees with the previous results using the numerical renormalization group as the impurity solver[9,33], and slave boson mean field theory,[6] and this is valid even far away from half-filling. The prefactor is, however, of the order of 1 only in the case of nearly half-filled featureless conduction band. Only in this case there is a single energy scale in the ALM and all additional low-energy scales assigned to different physical properties are proportional to this single low-temperature scale. For small occupation of c-electrons there are two energy scales: T_K^0 where the screening begins, and $T^* \ll T_K^o$ where coherence sets in.[9,33] $T^* \ll T_K^o$ also if there is a peak in the noninteracting conduction band density of states, while $T^* \gg T_K^o$ if there is a dip at the Fermi level.[6] Before we concentrate on the strength of inter-site correlations, which has not been previously explored, we will make few additional remarks about the analytical continuation performed in our work.

The only assumption that we use is that the self-energy is an analytical function, and we approximate the low-frequency part by a second order polynomial obtained from the self-energy at first three Matsubara frequencies. High frequency part of the self-energy is not important at all when calculating the resistivity, since the derivative of the Fermi-Dirac function in Eq. (4.1) is negligible away from the Fermi level. It is enough to keep the frequencies $|\omega| \lesssim 3T$ in the integral, and in this case a second order polynomial is a reasonable approximation for the self-energy. The approximation by a polynomial would be problematic if the self-energy is non-analytic near the quantum critical point. However, in our case we do not have such an irregular self-energy to worry about. Finally, our results include two stringent tests of the analytical continuation: the Fermi liquid behavior at low T is reproduced remarkably well, and the susceptibility data, which does not require the analytical continuation, give the same energy scales as obtained from the resistivity calculations. We emphasize, however, that our method for analytical continuation is not restricted to the Fermi liquid region, and we believe that it is the best possible option if we are interested only in the low frequency part of the spectrum. The maximum entropy method gives roughly correct spectra at intermediate frequencies, but from our experience, it never gives better results than the polynomial fit at low frequencies. The small noise from QMC data can also lead to pretty bad results in the Padé method for the analytical continuation.

V. STRENGTH OF NONLOCAL CORRELATIONS

The results obtained in the previous section are exact if the correlations are local, i.e. if the self-energy depends only on the frequency and not on the momentum. In order to determine the importance of nonlocal correlations we consider the ALM within CDMFT with two sites in a unit cell, as the minimal model which includes nonlocal correlations. We restrict to the paramagnetic solution. Typical results for the f-electron self-energy are shown in Fig. 7. The hybridization parameter in this figure is chosen very close to critical value $V = 0.18 \approx V_c$, but the results for the self-energy are qualitatively the same also for hybridization away from the critical point. The inter-site correlations are determined by the difference between even and odd components of the self energy, Σ_{00} and $\Sigma_{\pi\pi}$. At $T = 1/200$, Fig. 7(a), the self-energy fully coincides with the single site DMFT solution. At $T = 1/600$, Fig. 7(b), very weak inter-site correlations are present, and they gradually increase as the tempera-

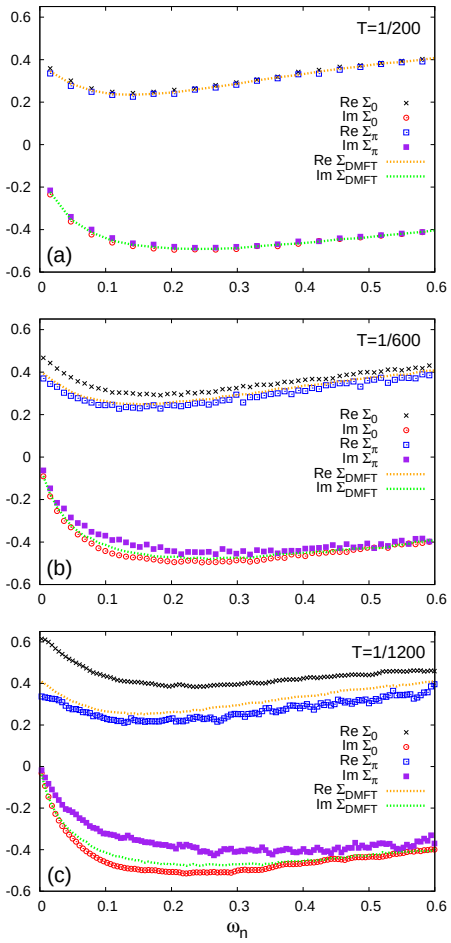

FIG. 7: (Color online) Comparison of the paramagnetic DMFT and CDMFT solution for the self-energy on the Matsubara axis for $V = 0.18$ and $T = 1/200, 1/600, 1/1200$.

ture is further lowered to $T = 1/1200$, Fig. 7(c). We note that we did not find any signatures of the Kondo breakdown - the decoupling of f-electrons and Fermi surface reconstruction for $V = V_c$.[34] The imaginary part of the self-energy $\mathrm{Im}\Sigma_f(\omega = 0)$ goes to zero, and the quasiparticle weight, $Z = (1 - \partial \mathrm{Im}\Sigma(i\omega)/\partial\omega)^{-1}|_{\omega\to 0^+} \sim 1/m^*$, remains finite as $T \to 0$ and $V = V_c$.

The strength of nonlocal correlations can be quantified using the probabilities for the occupation of different cluster eigenstates. At high temperatures, f-electrons are almost decoupled, and the probabilities P_s and P_t for the singlet and (one of three available) triplet states are almost the same, and approach to the free spin value $P_s \approx P_t \sim 0.25$. At low temperature the probability of the singlet state suddenly increases, and the singlet cluster eigenstate is dominantly occupied for $T \lesssim T_{nl}$. Large singlet probability P_s, which approaches to 1 at the lowest temperatures, implies strong singlet correlations. We can use these probabilities to define a crossover temperature T_{nl} which divides the regions of strong and weak

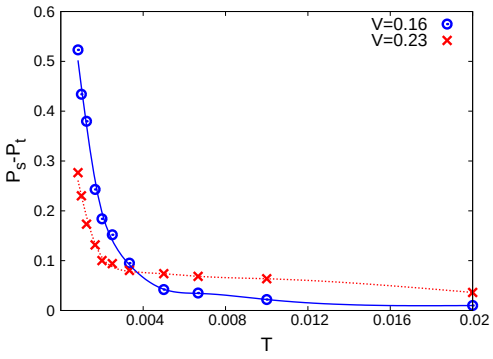

FIG. 8: (Color online) Difference of probabilities for finding the two-site impurity in the singlet and triplet cluster eigenstate.

inter-site correlations. We define T_{nl} as the temperature when $P_s - P_t = 0.1$, which is shown by a blue dotted line on the phase diagram, Fig. 1. T_{nl} roughly follows T_N, but stays large at the lowest temperatures also for $V > V_c$. The calculation of the observables, like the spin susceptibility and resistivity, remains to be done in the future work. While for reliable quantitative analysis we need to study also larger clusters and compare different clustering schemes since the two-site cluster version may overestimate the local singlet formation, we expect that the two impurity results already give a good estimate of the line which separates regions of strong and weak inter-site correlations.

VI. CONCLUSION AND DISCUSSION

In summary, we have solved CDMFT equations with two sites in a unit cell for nearly half-filled Anderson lattice model and compared the results with single-site DMFT. The phase diagram generally agrees with Doniach's physical picture: the antiferromagnetic phase is stabilized when RKKY interaction energy is larger than the Kondo temperature. The CDMFT solution gives much narrower AFM phase as compared to DMFT, which is expected since the mean-field solution generally overestimates a tendency to magnetic order, and two-site CDMFT overestimates the local singlet-formation, which competes with the long range magnetic order, hence the exact Néel temperature of the ALM is expected to be somewhere between the two limits. At temperatures above T_N the nonlocal correlations are small and the CDMFT and the DMFT paramagnetic solution are almost the same. This conclusion has important practical consequences for theoretical studies of heavy fermions. For temperatures larger then T_N the self-energy is weakly momentum-dependent, which explains the success of local LDA+DMFT approach in ab initio calculation of transport and thermodynamic properties of heavy fermions. Heavy fermions are particularly well

suited for the single-site DMFT approach since the interesting crossovers in transport and thermodynamic properties, from coherent to fully incoherent behavior, are seen in a broad temperature region above very low ordering temperature. At temperatures $T \lesssim T_N$ when short range processes are included, and if frustration at short distances is weak, the modifications from local DMFT predictions can be substantial.

We have also determined the lattice coherence temperature T^* from the resistivity and magnetic susceptibility calculated within DMFT and made a careful comaprison with the Kondo scale T_K^o for diluted impurities with the same set of parameters. The results clearly show that there exists a single energy scale $T^* \sim T_K^o$, which dominates the low temperature properties in the case of a nearly half-filled featureless conduction band. The comparison with the CDMFT solution shows that for stronger hybridization the nonlocal correlations are negligible at temperatures $T^*(V)$ and that T^* is approximately the same as given by the local DMFT solution. Near the quantum critical point, the inter-site correlations have to be properly taken into account to determine the lattice coherence scales. For this purpose, larger clusters and different clustering schemes also need to be considered, an important research direction which is left for future work. In real materials the effects of atomic multiplets and crystal fields, as well as the existence of sharp peaks or dips in the density of states at the Fermi level may significantly modify the low temperature physics[6,35] as compared to our simple model.

We note that in this work we have concentrated on a broad temperature range above the quantum critical point and have not directly addressed an important and controversial question of the nature of the quantum critical point.[12,34,36] Our two-site CDMFT solution, however, shows that f-electron density of states remains finite at the Fermi level even very near the critical point and we did not see signatures of the Kondo breakdown - decoupling of the f-electrons from the conduction bath at the Fermi level. This agrees with recent studies of the Kondo lattice model within dynamical cluster approximation,[37] and numerical renormalization group studies of two-impurity Anderson model.[38] Further study in this direction is needed, for different parameter regimes and larger clusters, facilitated with the CTQMC impurity solver which is proven to be able to reliably treat the competition of small energy scales.

Acknowledgments

We thank M. Ferrero and M. Vojta for usefull discussions. D.T. acknowledges support from the Serbian Ministry of Education and Science under project No. ON171017. K.H. was supported by NSF grant DMR-0746395, G.K. by NSF DMR-0906943, and V. D. by the National High Magnetic Field Laboratory and the NSF Grant DMR-1005751. D.T was supported in part by I2CAM Junior Exchange Award under NSF Grant DMR-0844115. D.T., K.H., and G.K. acknowledge the hospitality of KITP, Santa Barbara, under NSF Grant PHY05-51164. Numerical simulations were run on the AEGIS e-Infrastructure, supported in part by FP7 projects EGI-InSPIRE, PRACE-1IP and HP-SEE.

Appendix A: Self-consistency equations

In the CDMFT the original lattice is tiled with a superlattice of clusters and an effective Anderson impurity action is derived for a single cluster and supplemented by the self-consistency condition which relates the cluster Green's function to the local Green's function of the superlattice. The hybridization bath for the Anderson impurity action, the cluster Green function and the cluster self-energy have inter-site components and can be conveniently represented in the matrix form. For the cluster of two impurities the Green function takes the form

$$\hat{G}_f = \begin{pmatrix} G_{11\downarrow} & G_{12\downarrow} & 0 & 0 \\ G_{21\downarrow} & G_{22\downarrow} & 0 & 0 \\ 0 & 0 & G_{11\uparrow} & G_{12\uparrow} \\ 0 & 0 & G_{21\uparrow} & G_{22\uparrow} \end{pmatrix}. \quad \text{(A1)}$$

From the CDMFT self-consistency equation, the hybridization function $\hat{\Delta}$ is given by

$$\hat{\Delta}(i\omega_n) = i\omega_n + \mu - E_f - \hat{\Sigma}_f(i\omega_n) - \hat{G}_f^{-1}(i\omega_n), \quad \text{(A2)}$$

where the cluster Green function coincides with the local component of the lattice Green function

$$\hat{G}_f(i\omega_n) = \frac{1}{N}\sum_{\vec{k}} \hat{G}_f(i\omega_n, \vec{k}). \quad \text{(A3)}$$

$\hat{G}_f(i\omega_n, \vec{k})$ is easily obtained by integrating out the conduction electrons from the action which corresponds to the Hamiltonian (2.1) and its spin σ component is explicitly given by

$$\hat{G}_{f\sigma}(i\omega_n, \vec{k}) = \Big[\begin{pmatrix} i\omega_n + \mu - E_f & 0 \\ 0 & i\omega_n + \mu - E_f \end{pmatrix} - V^2 \left(i\omega_n + \mu - \hat{t}(\vec{k}) \right)^{-1} - \begin{pmatrix} \Sigma_{11\sigma} & \Sigma_{12\sigma} \\ \Sigma_{21\sigma} & \Sigma_{22\sigma} \end{pmatrix} \Big]^{-1} \quad \text{(A4)}$$

For a hypercubic lattice the summation over $\vec{k}$ is done in the reduced Brillouin zone: $k_x \in (-\frac{\pi}{2}, \frac{\pi}{2})$, $k_y, k_z \in (-\pi, \pi)$, and the hopping term is equal to

$$\hat{t}(\vec{k}) = \begin{pmatrix} 0 & e^{-ik_x}\varepsilon_{\vec{k}} \\ e^{ik_x}\varepsilon_{\vec{k}} & 0 \end{pmatrix}, \quad \text{(A5)}$$

with $\varepsilon_{\vec{k}} = -2t(\cos k_x + \cos k_y + \cos k_z)$.

We solve the two-site Anderson impurity problem using CTQMC impurity solver as implemented in Ref. 22.

This requires to switch to the cluster momenta basis functions, which are in the case of two sites in a cluster given by

$$|\psi_{0,\sigma}\rangle = (|\sigma,0\rangle + |0,\sigma\rangle)/\sqrt{2}$$
$$|\psi_{\pi,\sigma}\rangle = (|\sigma,0\rangle - |0,\sigma\rangle)/\sqrt{2} \quad \text{(A6)}$$

In this new basis, the hopping matrix is equal to

$$\hat{t}(\vec{k}) = \varepsilon_{\vec{k}} \begin{pmatrix} \cos k_x & i\sin k_x \\ -i\sin k_x & -\cos k_x \end{pmatrix}, \quad \text{(A7)}$$

and the self-consistency equation is given by

$$\begin{pmatrix} G_{00\sigma} & G_{0\pi\sigma} \\ G_{\pi 0\sigma} & G_{\pi\pi\sigma} \end{pmatrix} = \frac{1}{N}\sum_k \left[\begin{pmatrix} i\omega_n + \mu - E_f & 0 \\ 0 & i\omega_n + \mu - E_f \end{pmatrix} - V^2 \left(i\omega_n + \mu - \hat{t}(\vec{k})\right)^{-1} - \begin{pmatrix} \Sigma_{00\sigma} & \Sigma_{0\pi\sigma} \\ \Sigma_{\pi 0\sigma} & \Sigma_{\pi\pi\sigma} \end{pmatrix} \right]^{-1}, \quad \text{(A8)}$$

where

$$\left(i\omega_n + \mu - \hat{t}(\vec{k})\right)^{-1} = \frac{1}{(i\omega_n+\mu)^2 - \varepsilon_{\vec{k}}^2} \times \begin{pmatrix} i\omega_n + \mu + \varepsilon_{\vec{k}}\cos k_x & i\varepsilon_{\vec{k}}\sin k_x \\ -i\varepsilon_{\vec{k}}\sin k_x & i\omega_n + \mu - \varepsilon_{\vec{k}}\cos k_x \end{pmatrix} \quad \text{(A9)}$$

The components of the Green functions are related to those in the direct basis as

$$\begin{aligned} G_{00\sigma} &= (G_{11\sigma} + G_{22\sigma} + G_{21\sigma} + G_{12\sigma})/2, \\ G_{0\pi\sigma} &= (G_{11\sigma} - G_{22\sigma} + G_{21\sigma} - G_{12\sigma})/2, \\ G_{\pi 0\sigma} &= (G_{11\sigma} - G_{22\sigma} - G_{21\sigma} + G_{12\sigma})/2, \\ G_{\pi\pi\sigma} &= (G_{11\sigma} + G_{22\sigma} - G_{21\sigma} - G_{12\sigma})/2. \end{aligned} \quad \text{(A10)}$$

In the AFM phase $G_{11\uparrow} = G_{22\downarrow}$, $G_{22\uparrow} = G_{11\downarrow}$, $G_{12\uparrow} = G_{21\downarrow}$, and $G_{21\uparrow} = G_{12\downarrow}$. Therefore, $G_{00\uparrow} = G_{00\downarrow}$, $G_{\pi\pi\uparrow} = G_{\pi\pi\downarrow}$, $G_{0\pi\uparrow} = -G_{0\pi\downarrow}$, and $G_{\pi 0\uparrow} = -G_{\pi 0\downarrow}$. Also, the off-diagonal Green's functions at constant spin are the same, $G_{0\pi\uparrow} = G_{\pi 0\uparrow}$ and $G_{0\pi\downarrow} = G_{\pi 0\downarrow}$. Analogous relations are valid for the self-energy and for the hybridization bath. Therefore, the effective two-impurity Anderson model is solved in the hybridization bath with three independent components

$$\hat{\Delta} = \begin{pmatrix} \Delta_{00} & \Delta_{0\pi} & 0 & 0 \\ \Delta_{0\pi} & \Delta_{\pi\pi} & 0 & 0 \\ 0 & 0 & \Delta_{00} & -\Delta_{0\pi} \\ 0 & 0 & -\Delta_{0\pi} & \Delta_{\pi\pi} \end{pmatrix}, \quad \text{(A11)}$$

and supplemented by the self-consistency condion, Eqs. (A2) and (A8). The Green's function also has three independent components

$$\begin{aligned} G_{00} &= (G_{11} + G_{22})/2 + G_{12}, \\ G_{0\pi} &= (G_{11} - G_{22})/2, \\ G_{\pi\pi} &= (G_{11} + G_{22})/2 - G_{12}, \end{aligned} \quad \text{(A12)}$$

where the spin index has been suppressed. Analogous relations are valid for the self-energy. We note that the off-diagonal components $\Delta_{0\pi}$ lead to the antiferromagnetic order. In the paramagnetic solution they are equal to zero.

Appendix B: Green's functions in the AFM solution

Typical results for the f-electron self-energy and Green's function in the AFM phase are given in Fig. 9. The self-energy, Fig. 9(a), has very small nonlocal component $\Sigma_{12} = (\Sigma_{00} - \Sigma_{\pi\pi})/2$. Finite $\Sigma_{0\pi}$ component leads to the staggered magnetization. The corresponding local Green's function, $G_{11,\sigma} = (G_{00,\sigma} + G_{\pi\pi,\sigma})/2 + G_{0\pi,\sigma}$, has different spin up and spin down components, Fig. 9(b). For given parameters, $n_{f\uparrow} - n_{f\downarrow} = 0.35$, $n_{c\uparrow} - n_{c\downarrow} = -0.08$, $n_{f\uparrow} + n_{f\downarrow} = 0.96$, and the total occupation is 1.92.

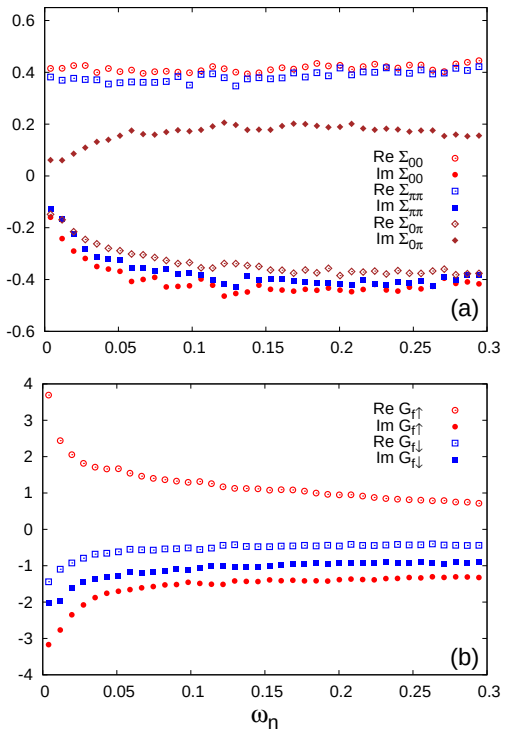

FIG. 9: (Color online) Self-energy (a) and local Green's function (b) in CDMFT solution for $V = 0.16$ and $T = 1/800$.

We note that the Néel temperature strongly depends on the occupation number. It is the highest in the Kondo insulator (for $n_f + n_c = 2$), and drops sharply as the occupation number decreases. In the Kondo insulator for $V = 0.18$, $E_f = -0.6$, we find that $T_N^{DMFT} \approx 0.015$, which is similar as in Ref. 13, while $T_N^{CDMFT} \approx 0.004$. We suspect that T_N is much larger in Ref. 23 because the solution gets stuck in a metastable local minimum, giving false higher value for T_N, or because of the self-consistency condition, which is in fact different in Ref. 23. The expression for the Green function in Ref. 23 includes periodized self-energy which may be noncausal. In our work, we use standard CDMFT implementation of the cluster DMFT.

[1] A. C. Hewson, *The Kondo Problem to Heavy Fermions* (Cambridge University Press, Cambridge, 1997).
[2] G. R. Stewart, Rev. Mod. Phys. **56**, 755 (1984).
[3] H. von Löhneysen, A. Rosch, M. Vojta, and P. Wölfle, Rev. Mod. Phys. **79**, 1015 (2007).
[4] Y.-F. Yang, Z. Fisk, H.-O. Lee, J. D. Thompson, and D. Pines, Nature **454**, 611 (2008).
[5] S. Nakatsuji, D. Pines, and Z. Fisk, Phys. Rev. Lett. **92**, 016401 (2004).
[6] S. Burdin and V. Zlatić, Phys. Rev. B **79**, 115139 (2009).
[7] M. W. McElfresh, M. B. Maple, J. O. Willis, Z. Fisk, J. L. Smith, and J. D. Thompson, Phys. Rev. B **42**, 6062 (1990).
[8] J. D. Thompson and Z. Fisk, Phys. Rev. B **31**, 389 (1985).
[9] C. Grenzebach, F. B. Anders, G. Czycholl, and T. Pruschke, Phys. Rev. B **74**, 195119 (2006).
[10] H. Hegger, C. Petrovic, E. G. Moshopoulou, M. F. Hundley, J. L. Sarrao, Z. Fisk, and J. D. Thompson, Phys. Rev. Lett. **84**, 4986 (2000).
[11] C. Petrovic, P. G. Pagliuso, M. F. Hundley, R. Movshovich, J. L. Sarrao, J. D. Thompson, Z. Fisk, and P. Monthoux, J. Phys.: Condens. Matter **13**, L337 (2001).
[12] P. Gegenwart, Q. Si, and F. Steglich, Nat. Phys. **4**, 186 (2008).
[13] A. N. Tahvildar-Zadeh, M. Jarrell, and J. K. Freericks, Phys. Rev. B **55**, R3332 (1997).
[14] A. Georges, G. Kotliar, W. Krauth, and M. J. Rozenberg, Rev. Mod. Phys. **68**, 13 (1996).
[15] G. Kotliar, S. Y. Savrasov, G. Pálsson, and G. Biroli, Phys. Rev. Lett. **87**, 186401 (2001).
[16] T. Maier, M. Jarrell, T. Pruschke, and M. H. Hettler, Rev. Mod. Phys. **77**, 1027 (2005).
[17] J. H. Shim, K. Haule, and G. Kotliar, Science **318**, 1615 (2007).
[18] H. C. Choi, B. I. Min, J. H. Shim, K. Haule, and G. Kotliar, arXiv:1105.2402 (2011).
[19] S. V. Streltsov, E. Gull, A. O. Shorikov, M. Troyer, V. I. Anisimov, and P. Werner, arXiv:1106.3470 (2011).
[20] G. Kotliar, S. Y. Savrasov, K. Haule, V. S. Oudovenko, O. Parcollet, and C. A. Marianetti, Rev. Mod. Phys. **78**, 865 (2006).
[21] P. Werner, A. Comanac, L. de Medici, M. Troyer, and A. J. Millis, Phys. Rev. Lett. **97**, 076405 (2006).
[22] K. Haule, Phys. Rev. B **75**, 155113 (2007).
[23] P. Sun and G. Kotliar, Phys. Rev. Lett. **95**, 016402 (2005).
[24] L. De Leo, M. Civelli, and G. Kotliar, Phys. Rev. B **77**, 075107 (2008).
[25] J. Otsuki, H. Kusunose, and Y.Kuramoto, Phys. Rev. Lett. **102**, 017202 (2009).
[26] H. Schweitzer and G. Czycholl, Phys. Rev. Lett. **67**, 3724 (1991).
[27] E. Miranda, V. Dobrosavljević, and G. Kotliar, J. Phys.: Condens. Matter **8**, 9871 (1996).
[28] O. Gunnarsson, M. Calandra, and J. E. Han, Rev. Mod. Phys. **75**, 1085 (2003).
[29] N. E. Hussey, K. Takenaka, and H. Takagi, Philos. Mag. **84**, 2847 (2004).
[30] We note that in half-filled Mott-Hubbard systems[39] the resistivity can exceed the Mott-Ioffe-Regel limit by more than an order of magnitude due to the appearance of the pseudogap at the Fermi level.
[31] A. C. Jacko, J. O. Fjærestad, and B. J. Powell, Nat. Phys. **5**, 422 (2009).
[32] K. Kadowaki and S. B. Woods, Solid State Commun. **58**, 507 (1986).
[33] T. Pruschke, R. Bulla, and M. Jarrell, Phys. Rev. B **61**, 12799 (2000).
[34] T. Senthil, M. Vojta, and S. Sachdev, Phys. Rev. B **69**, 035111 (2004).
[35] A. H. Nevidomskyy and P. Coleman, Phys. Rev. Lett. **103**, 147205 (2009).
[36] W. Knafo, S. Raymond, P. Lejay, and J. Flouquet, Nat. Phys. **5**, 753 (2009).
[37] L. C. Martin, M. Bercx, and F. F. Assaad, Phys. Rev. B **82**, 245105 (2010).
[38] L. Zhu and J. X. Zhu, Phys. Rev. B **83**, 195103 (2011).
[39] M. M. Radonjić, D. Tanasković, V. Dobrosavljević, and K. Haule, Phys. Rev. B **81**, 075118 (2010).